Experimental and Numerical Study on the Fracture Behaviour of the Aluminium Alloy AA7075-T651

O.S. Hopperstad[1], K.O. Pedersen[2] and T. Børvik[1,3]

[1]Structural Impact Laboratory (SIMLab) and Department of Structural Engineering, Norwegian University of Science and Technology, NO-7491 Trondheim, Norway

[2]SINTEF Materials & Chemistry, NO-7465 Trondheim, Norway

[3]Norwegian Defence Estates Agency, Research & Development Department, NO-0103 Oslo, Norway

The fracture mechanisms of AA7075-T651 were studied by material tests at various stress states and loading directions, plate impact tests and fractographic investigations. A combination of transgranular and intergranular fracture was observed, and delamination in the rolling plane of the plate was found for high stress triaxiality. In the plate impact tests, delamination and fragmentation were seen at the macroscopic level, while at the microscopic level the fracture mechanisms resemble those found in the material tests. Based on the material test data, a constitutive relation and a fracture criterion were determined for the alloy. Finite element simulations of the plate impact tests reproduced the failure modes found in the experiments with reasonable accuracy.

1. Introduction

In the design of protective structures against ballistic impact, the material strength is an important parameter. The high-strength aluminium alloy AA7075 is attractive for use in lightweight protective structures due to its excellent strength-to-weight ratio. However, since fragments generated from the protective structure may be a serious hazard for both personnel and equipment, adequate ductility of the material should be ensured.

The fracture behaviour of high strength, age hardening aluminium alloys has been extensively studied during the last several decades [1]-[10]. Age hardening aluminium alloys form precipitates, precipitation free zones, grain boundary precipitates and grains with different shapes during processing. The grains can either be equiaxed, obtain a pancake shape or be elongated in the deformation direction. The grain structure and the crystallographic texture will affect the fracture behaviour. A competition between intergranular and transgranular fracture occurs in materials that have shearable precipitates and where precipitation free zones are formed adjacent to the grain boundaries. If the material contains high amount of coarse intermetallic particles, nucleation, growth and coalescence of voids from these particles will also be an important fracture mechanism. Particle stringers which are often seen in rolled and extruded materials will enhance this latter effect.

The aim of this paper is to study the quasi-static and dynamic fracture behaviour of the rolled aluminium alloy AA7075-T651. To this end, quasi-static and dynamic material tests and plate impact tests have been conducted [11]. The fracture mechanisms are investigated with respect to grain morphology, dimple structure and intermetallic coarse particles. On the basis of the quasi-static and dynamic material tests, a thermoelastic-thermoviscoplastic constitutive model and a ductile fracture criterion were determined for AA7075-T651, and finite element analyses of the plate impact tests were carried out using the explicit solver of LS-DYNA [12]. Delamination and fragmentation of the target occurred in the plate impact tests, and these failure modes were reasonably well captured in the simulations.
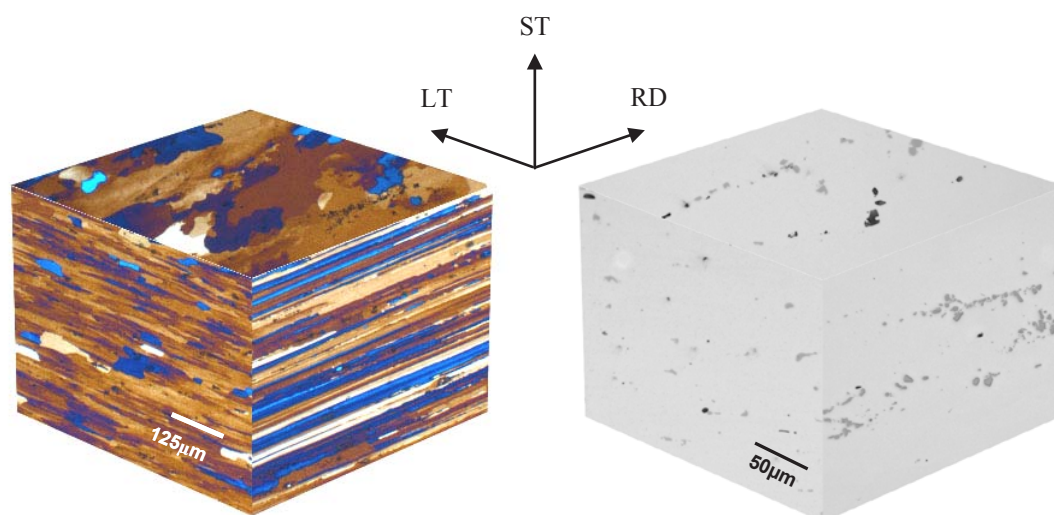
Fig. 1 Tri-planar optical micrographs illustrating the grain structure (left) and the particle distribution (right) of the AA7075-T651 aluminium alloy.

2. Material and experimental procedures

Rolled plates of the aluminium alloy AA7075 in T651 temper are investigated. Temper T651 implies that the alloy is slightly stretched and aged to peak strength. The 20 mm thick plate has nominal yield and tensile strengths of 505 and 570 MPa, respectively. The nominal chemical composition of the AA7075 alloy is (in wt%): 0.06 Si, 0.19 Fe, 1.3 Cu, 0.04 Mn, 2.4 Mg, 0.19 Cr, 5.7 Zn, 0.08 Ti, 0.15 other elements and Al balance.

Four series of material tests have been performed at ambient temperature. Only results from the quasi-static tensile tests on smooth and notched axisymmetric specimens will be discussed here. The smooth specimens had tensile axis oriented 0°, 45° and 90° with respect to the rolling direction of the plate. The notched axisymmetric specimens had notch radius 0.8 and 2.0 mm and the tensile axis was in the rolling direction. Plate impact tests were carried out in a compressed gas-gun. The target plates with dimension 600×600 mm^2 and nominal thickness of 20 mm were clamped in a 500 mm diameter circular frame. Hardened steel projectiles (20 mm diameter, 197 g mass, 52 HRC) with blunt and ogival nose shapes were used. The projectiles were launched at impact velocities just below and well above the ballistic limit velocity of the plate. The impact event was captured by a digital high-speed video camera operating at a constant framing rate of 50.000 fps. Impact and residual velocities were measured using laser-based optical devices and the high-speed camera system. The reader is referred to [11] for detailed information on the mechanical tests.

The microstructure of the AA7075-T651 material was characterised by standard metallographic preparation techniques. The distribution and the morphology of the coarse particles were investigated by first grinding the samples on progressively finer grades of SiC emery paper up to 1200 mesh and then polishing the surface using 1 μm diamond paste. Finally, the specimens were chemical/mechanical polished using an active oxide suspension to obtain a smooth and scratch-free surface. The grain structure before and after deformation to fracture was unveiled by anodising the ground and polished specimens using 5% fluoroboric acid (HBF$_4$) for 2 minutes and an applied voltage of 15-20V at room temperature. The specimens were investigated in an optical microscope with polarised light. Sections in all three orthogonal directions of the rolled plate were investigated. The fracture surfaces were investigated in a scanning electron microscope (Zeiss 55VP FEG) equipped with a digital camera.
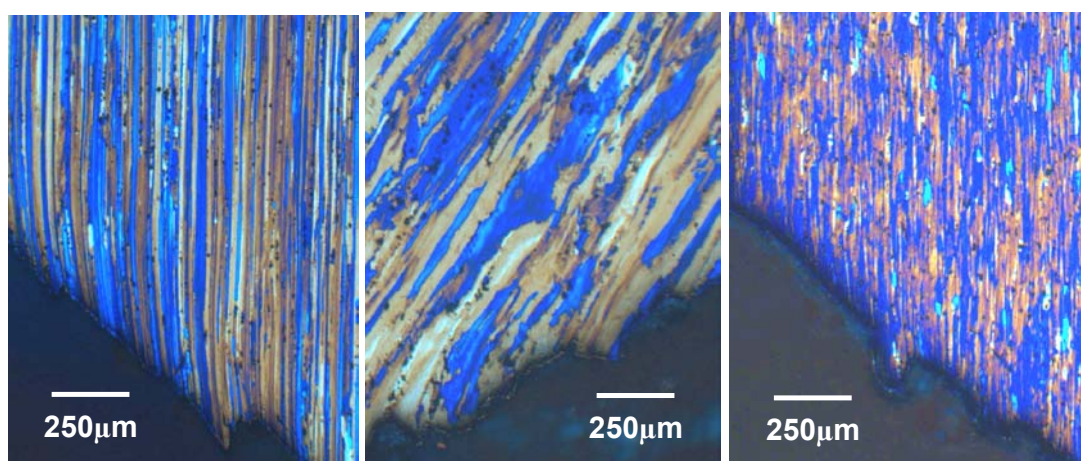
Fig. 2 Optical micrographs of longitudinal mid-section at the fracture location in tensile tests on smooth axisymmetric specimens in the rolling direction (0°), the 45° direction and the long transverse direction (90°) (from left to right).

3. Experimental results

The grain structure of the as-received AA7075 alloy is shown in Fig. 1 (left) as tri-planar optical micrographs along the three orthogonal directions of the rolled plate. The main feature is the deformed, fibrous and non-recrystallised grain structure caused by the rolling deformation. Coarse recrystallised grains are observed in-between the deformed structure. The recrystallised grains have an irregular, elongated shape and are flattened in the rolling direction. Due to the rolling, the grain morphology is different in the three orthogonal directions. The intermetallic particle distribution for this alloy is well documented in [13], while the variations in shape and size in the three different orthogonal directions are displayed in [14]. The primary particles consist mainly of iron rich and silicon-based intermetallic particles, and are shown for this material as tri-planar optical micrographs in Fig. 1 (right). The constitutive particles are relatively large [13] and are gathered in clusters. They are more or less elongated in the rolling direction as can be seen in the longitudinal plane. Micrographs taken in the transverse plane indicate that the particles are nearly equiaxed and evenly distributed which is not the case when observed in the two other planes (rolling plane and longitudinal plane). Dispersoids inhibiting recrystallisation are also formed in these alloys during homogenisation and are evenly distributed in the grains [15]. A high density of the hardening phase η' in the interior of the grain and grain boundary precipitates η are present. Near the grain and sub-grain boundaries precipitation free zones are formed. These zones are softer than the matrix and are prone to strain localisation during deformation.

The crack path and how the cracks are growing compared to the grain structures are shown in Fig. 2 for the tensile tests with three different orientations. At a macroscopic level the fracture seems to appear in a shear mode about 45° to the longitudinal axis for all three orientations. However, on a lower scale it becomes apparent that the fracture path is partly along the grain boundary and partly through the grain. The recrystallised grains seem to contribute only modestly to the fracture behaviour since they are seen neither along the crack path nor in the fracture surface.

Scanning electron micrographs of the fracture surface from the tensile tests in the 90° direction are presented in Fig. 3. The figure shows both the secondary and backscatter electron micrographs to reveal the dimple structure and the particle distribution. The fracture surface consists of grain facets which are decorated with small precipitates and areas of transgranular fracture with high density of dimples. In addition, primary intermetallic stringers are located in the fracture surface for the 90° orientation. Elongated and cracked particles in the bottom of voids underline the importance of the primary particles on the fracture behaviour of the material, as voids are nucleated at the locations of these particles.
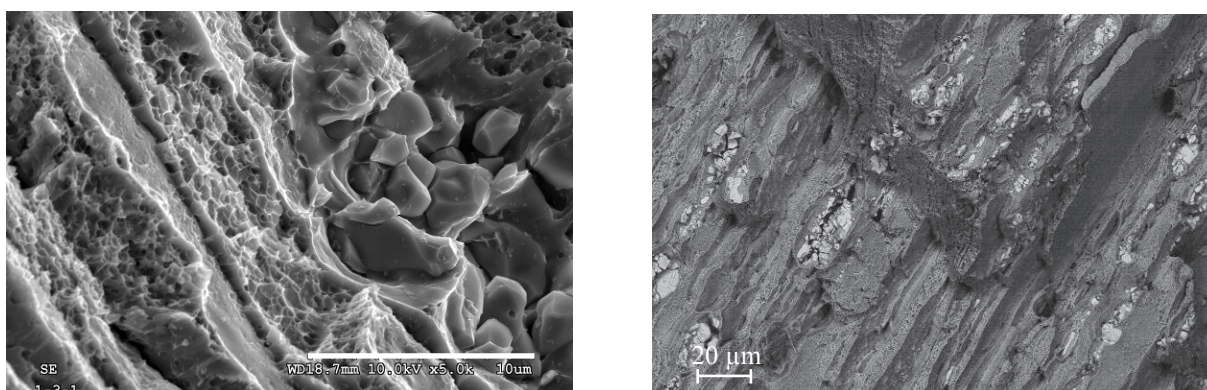
Fig. 3 Scanning electron micrographs of fracture surface from tensile tests on smooth axisymmetric specimen in the long transverse direction (90°): Secondary electron micrograph (left) and backscatter electron micrograph (right).
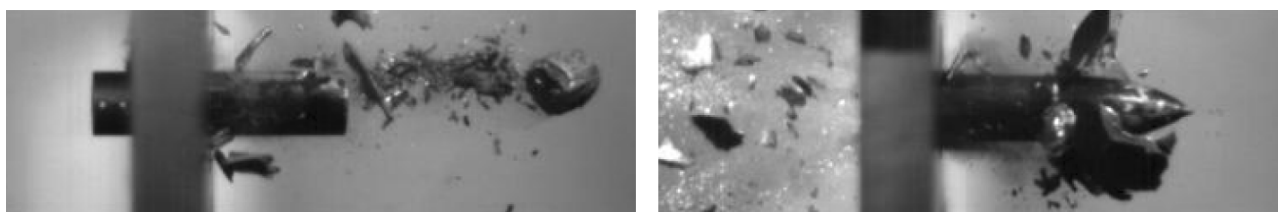

Fig. 4 Perforation of the 20 mm thick AA7075-T651 target plate by a projectile having 20 mm diameter, 197 gram mass and blunt nose shape (left) or ogival nose shape (right) [11].

Three classes of dimples were observed in the fracture surfaces. These are large-sized dimples caused by the coarse intermetallic particles, medium-sized dimples due to the grain-boundary precipitates and small-sized dimples nucleated on the high density of fine intermetallic particles.

Introducing a notch in the tensile specimen increases the stress triaxiality in the deformation zone and leads to secondary cracks along the rolling plane. The secondary cracks seem to have the character of delamination along the boundaries of the flat and elongated grains in the rolling plane. While notched specimens reveal the same microscopic fracture appearance as the smooth specimens, the higher triaxiality increases the effect of the grain boundaries on the fracture behaviour, leading to the secondary cracks in the rolling plane. The grain boundaries, or the regions in the vicinity of the grain boundaries, are weak areas because of the precipitation free zones and the grain boundary particles. In the rolling plane, the grains have a flat and elongated appearance and the distance between the grain nodes is large. Therefore, a crack can grow easily in or near the grain boundary (e.g. in the precipitation free zones) without any resistance from the grain nodes.

The perforation of the 20 mm thick AA7075-T651 target plate by blunt and ogival projectiles is shown in Fig. 4. It is seen that fragmentation occurs during impact for both projectiles, indicating a quasi-brittle behaviour of the alloy. The fragmentation is more extensive for the ogival projectile. Fig. 5 shows cross-sections through plates impacted by a blunt projectile (left) and an ogival projectile (right). The blunt projectile results in shear deformations and secondary cracks normal to the penetration channel. These cracks follow the grain boundaries and results in fragmentations due to high tensile stresses. Significant shear deformation is observed in the penetration channel far from the fragmentation zone. For an ogival projectile the shear deformation is less distinct. However, tensile stresses lead to delamination in the rolling plane, owing to the inhomogeneous and layered microstructure of the material. The result is the extensive fragmentation seen in Fig. 4. On a lower scale, the fracture appearance for both projectiles is similar and the main fracture mode is a combination of intergranular and transgranular fracture.
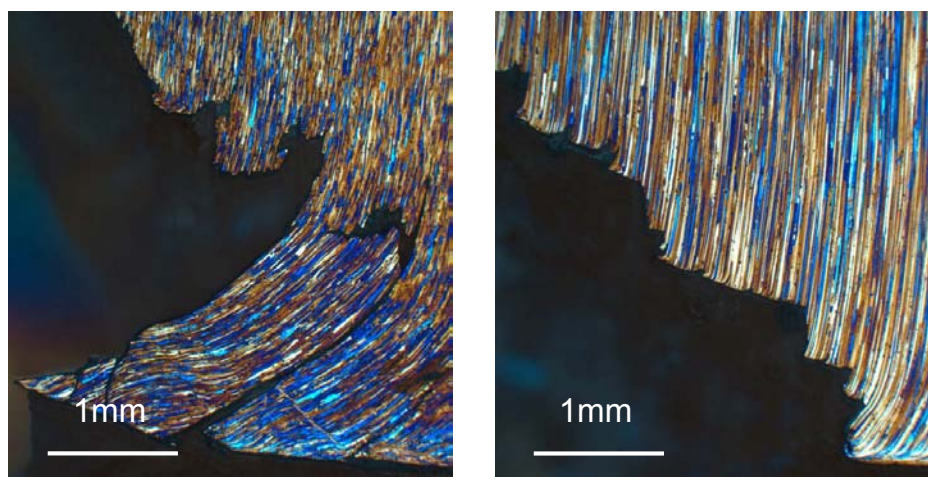
Fig. 5 Optical micrographs of sections within the fragmentation area of the cavities from the plate impact tests with blunt projectile (left) and ogival projectile (right).

4. Finite element simulations

The plate impact tests were analysed using the explicit solver of the non-linear finite element code LS-DYNA [12]. The material was modelled using an isotropic thermoelastic-thermoviscoplastic constitutive model and a simple one-parameter fracture criterion [11]. In the simulations presented here eight-node constant-stress solid elements with stiffness-based hourglass control were applied, while contact was modelled using an eroding surface-to-surface algorithm. The element size in the impact region was taken equal to $0.5 \times 0.5 \times 0.8$ mm^3, giving 25 elements through the thickness. To save computational time, the mesh was coarsened towards the fully clamped boundary using tetrahedral transition elements, and in the global part of the plate 7 elements were used over the target thickness. The resulting finite element models had about 330 000 elements and 850 000 nodes.

Simulations of the perforation process with blunt and ogival projectiles are shown in Fig. 6. Ogival projectiles perforate the plate by ductile hole-enlargement, while for blunt projectiles the perforation process is controlled by adiabatic shear localization. For both projectile shapes the quasi-brittle behaviour during perforation seen experimentally (see Fig. 4) is partly captured in the simulations. However, the simulations are not fully capable of capturing the extensive delamination and fragmentation of the plate seen experimentally and the impact velocity required to perforate the plate (or the ballistic limit velocity) tends to be overestimated. The reader is referred to [11] for more details on the finite element modelling of the plate impact tests and further comparison with the experimental results.

5. Concluding remarks

The fracture mechanisms of AA7075-T651 under quasi-static and dynamic loading conditions were investigated. A combination of transgranular and intergranular fracture was observed under quasi-static tensile loading, and delamination in the rolling plane was found for high stress triaxiality. In the plate impact tests, delamination and fragmentation were seen at the macroscopic level, while at the microscopic level, the fracture mechanisms resemble those found in the material tests. Finite element simulations of the plate impact tests, using a thermoelastic-thermoviscoplastic constitutive relation and simple one-parameter fracture criterion, were carried out. The simulations were found to reproduce the failure modes found in the experiments with reasonable accuracy.
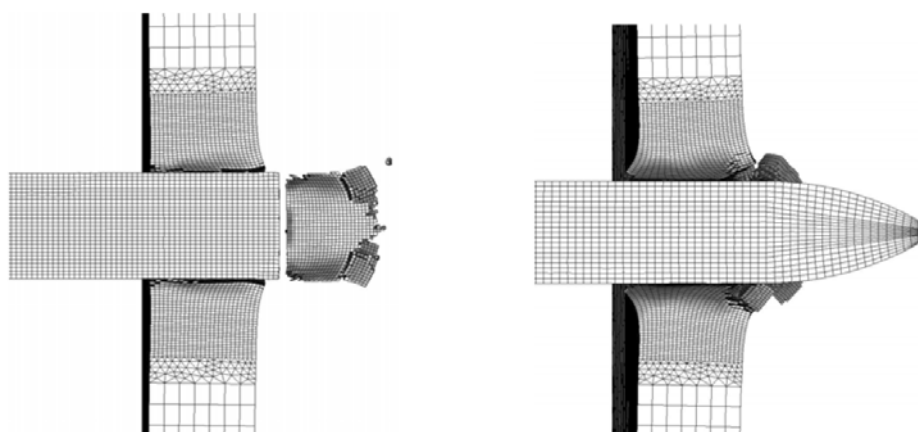
Fig. 6 Perforation of 20 mm thick AA7075-T651 plates by blunt (left) and ogival (right) projectiles in finite element simulations with solid elements. The fringe levels show the accumulated plastic strain in the range 0 (light gray) to 0.5 (dark gray). The 3D model has been sectioned through the centre to better show the perforation process.

References

[1] R.E. Zinkham: Eng. Fract. Mech. 1 (1968) 275-289.
[2] P.N.T. Unwin and G.C. Smith GC: J. Inst. Metals 97 (1969) 299-310.
[3] J.D. Embury and E. Nes: Z. Metallkd. 64 (1973) 805-812.
[4] J.D. Embury and E. Nes: Z. Metallkd. 65 (1974) 45-55.
[5] T. Kawabata and O. Izumi: Acta Metall. 24 (1976) 817-825.
[6] T. Kawabata and O. Izumi: Acta Metall. 25 (1977) 505-512.
[7] D. Dumont, A. Deschamps and Y. Brechet: Mater. Sci. Eng. A356 (2003) 326-336.
[8] D. Dumont, A. Deschamps and Y. Brechet: Acta Mater. 52 (2004) 2529-2540.
[9] T.S. Srivatsan, G. Guruprasad and V.K. Vasudevan: Mater. Des. 29 (2008) 742-751.
[10] K.O Pedersen, H.J. Roven, O.-G. Lademo and O.S. Hopperstad: Mater. Sci. Eng. A473 (2008) 81-89.
[11] T. Børvik, O.S. Hopperstad and K.O. Pedersen: Int. J. Impact Eng. 37 (2010) 537-551.
[12] LSTC. LS-DYNA Keyword User's Manual, Version 971. Livermore Software Technology Corporation, May, 2007
[13] N. Birbilis, M.K. Cavanaugh, R.G. Buchheit, D.G. Harlow DG and R.P. Wie: Mater. Sci. Technol. 1 (2005) 57-67.
[14] J.B. Jordon, M.F. Horstemeyer, K. Solanki, J.D. Bernard, J.T. Berry and T.N. Williams: Mater. Sci. Eng. A527 (2009) 169-178.
[15] I.J. Polmear: Light alloys – From traditional alloys to nanocrystals. Fourth edition. Elsevier 2006.